Urban-rural interactions in a South Korean forest in ozone and oxygenated volatile organic compound formation perspectives

[1]Saewung Kim, [2]So-Young Kim, [3]Meehye Lee, [3]Heeyoun Shim, [4,5]Glenn M. Wolfe, [6]Alex B. Guenther, and [1]Amy He, [2]Youdeog Hong, [2]Jinseok Han

1 Department of Earth System Science, School of Physical Sciences, University of California, Irvine, Irvine California, 92697 U.S.A.
2 National Institute Environmental Research, Incheon, South Korea
3 Department of Earth and Environmental Sciences, Korean University, Seoul, South Korea
4 Joint Center for Earth Systems Technology, University of Maryland Baltimore County, Baltimore, MD, USA
5 Atmospheric Chemistry and Dynamics Laboratory, NASA Goddard Space Flight Center, Greenbelt, MD, USA
6 Atmospheric Sciences and Global Change Division, Pacific Northwest National Laboratory, Richland WA USA

To be submitted to Atmospheric Chemistry and Physics “East Asian Megacity” Special Issue

Abstract

Rapid urbanization and economic development in East Asia in past decades has led to photochemical air pollution problems such as excess photochemical ozone and aerosol formation. Asian megacities such as Seoul, Tokyo, Shanghai, Gangzhou, and Beijing are surrounded by densely forested areas and recent research has consistently demonstrated the importance of biogenic volatile organic compounds (VOCs) from vegetation in determining oxidation capacity in the suburban Asian megacity regions. Uncertainties in constraining tropospheric oxidation capacity, dominated by hydroxyl radical, undermine our ability to assess regional photochemical air pollution problems. We present an observational dataset of CO, NO_X, SO_2, ozone, HONO, and VOCs (anthropogenic and biogenic) from Taehwa Research Forest (TRF) near the Seoul Metropolitan Area (SMA) in early June 2012. The data show that TRF is influenced both by aged pollution and fresh BVOC emissions. With the dataset, we diagnose HOx (OH, HO_2, and RO_2) distributions calculated using the University of Washington Chemical Box Model (UWCM v 2.1) with near-explicit VOC oxidation mechanisms from MCM 3.2 (The Master Chemical Mechanism). Uncertainty from unconstrained HONO sources and radical recycling processes highlighted in recent studies is examined using multiple model simulations with different model constraints. The results suggest that 1) different model simulation scenarios cause systematic differences in HO_X distributions especially OH levels (up to 2.5 times) and 2) radical destruction (HO_2+HO_2 or HO_2+RO_2) could be more efficient than radical recycling (HO_2+NO) especially in the afternoon. Implications of the uncertainties in radical chemistry are discussed with respect to ozone-VOC-NO_X sensitivity and VOC oxidation product formation rates. Overall, the VOC limited regime

69 in ozone photochemistry is assessed but the degree of sensitivity can significantly vary
70 depending on the model scenarios. The model results also suggest that RO_2 levels are
71 positively correlated with oxygenated VOCs (OVOCs) production that is not routinely
72 constrained by observations. These unconstrained OVOCs can cause higher than
73 expected OH loss rates (missing OH reactivity) and secondary organic aerosol formation.
74 The series of modeling experiments constrained by observations strongly urge
75 observational constraint of the radical pool to enable precise understanding of regional
76 photochemical pollution problems in the East Asian megacity region.

1. Introduction

NOx ($NO+NO_2$) and volatile organic compounds (VOCs) are two important precursors that drive HOx radical cycles(Levy, 1971). In the presence of NO_X, VOC oxidation processes recycle OH and produce photochemical oxidation products such as ozone and oxygenated VOCs (OVOCs). This reaction cycle is highly non-linear. For example, excess NO_2 may expedite nitric acid formation (R1), limiting ozone production. In the same context, excess VOCs may expedite peroxy radical production (R2), which limits OH regeneration from peroxy radicals.

$$OH + NO_2 + M \rightarrow HNO_3 + M \quad (R1)$$

$$HO_2 + RO_2 \rightarrow ROOH \quad (R2)$$

The non-linearity in tropospheric photochemistry has been relatively well studied in the urban regions of developed countries and applied in ozone reduction policy. The Los Angeles Metropolitan Area has accomplished significant ozone reduction by implementing aggressive emission reductions of both NOx and VOC especially from mobile sources (Ryerson et al., 2013). The remarkable ozone abatement was possible due to the fact that there is no significant pollution transport from other metropolitan areas and no significant natural emission sources especially volatile organic compounds from vegetation (BVOCs; biogenic volatile organic compounds) compared with anthropogenic VOC mostly from mobile sources (Pollack et al., 2013;Huang et al., 2013). In the late 80s, Trainer et al. (1987) first demonstrated the importance of isoprene (C_5H_8) as a peroxy radical source that can contribute significant ozone production in rural areas. The

100 importance of isoprene in ozone production in urban areas has also been highlighted, e.g.
101 in the Atlanta Metropolitan Area (Chameides et al., 1988).
102 Isoprene is a hemiterpenoid species and is the globally dominant VOC emission
103 from vegetation (Arneth et al., 2011;Guenther, 2013). Arguably, isoprene is the most
104 frequently studied BVOC from the perspective of atmospheric oxidation processes and
105 their implications for ozone and aerosol formation. However, significant uncertainty
106 hinders assessing the roles of isoprene in regional and global photochemistry in three
107 fronts. First, there is still significant uncertainty in estimating emission rates from each
108 individual plant species on regional scales (Guenther, 2013). Second, limited isoprene
109 inter-comparison results (Barket et al., 2001) suggest that there are large systematic
110 biases among different analytical techniques. Lastly, recent laboratory, theoretical and
111 field observations suggest significant uncertainty in tropospheric isoprene oxidation
112 processes initiated by OH. Until early 2000, it was thought that three first generation
113 isoprene oxidation products (methyl vinyl ketone, methacrolein, and formaldehyde) from
114 OH oxidation were enough to constrain isoprene tropospheric oxidation processes for
115 modeling purposes (e.g. Spaulding et al. (2003) and references therein). This is an
116 interesting evolution of thoughts considering that Paulson and Seinfeld (1992), one of
117 pioneering works describing isoprene oxidation, clearly claimed that 22 % of first
118 generation isoprene oxidation products from the reaction with OH was not identified and
119 likely included multifunctional C5 compounds. Recent advances in analytical techniques
120 (Kim et al., 2013a) have shown that indeed significant C5-hydroxy carbonyl (e.g.
121 isoprene hydroperxyenals, HPALD) and peroxide compounds are produced as first
122 generation isoprene oxidation products (Crounse et al., 2011;Paulot et al., 2009;Wolfe et

al., 2012;Zhao and Zhang, 2004). The product yields appeared to be a strong function of NO concentrations (Peeters and Muller, 2010). In general, at low to intermediate NO levels (~ 100 pptv or lower), the yields of C5-hydroxy carbonyl compounds become higher. These new findings in the isoprene oxidation process are also closely related with recent findings in unexpectedly high OH concentrations (Hofzumahaus et al., 2009;Lelieveld et al., 2008) and substantial missing OH sinks also known as unexpectedly high OH reactivity in high isoprene environments (Di Carlo et al., 2004;Edwards et al., 2013;Kim et al., 2011;Lou et al., 2010).

These new findings have significant implications for regional air quality especially regarding photochemical ozone and SOA production. Despite the strong anthropogenic pollutant emissions in East Asia (China, Japan and South Korea), recent research has shown that isoprene accounts for a major OH chemical sink in suburban areas near Beijing (Ran et al., 2011), the Pearl River Delta region (Lu et al., 2012), Taipei, Taiwan (Chang et al., 2014) and Seoul (Kim et al., 2013d;Kim et al., 2013b). Consequently, modeling studies also clearly show that isoprene contributes significantly to ozone formation in Asian megacity regions. Kim et al. (2013d) reported that simulated ozone levels with isoprene chemistry are up to 30 % higher than ozone simulation without isoprene chemistry using the WRF-Chem model, indicating an urgent need to implement improved isoprene chemistry schemes in these models in order to simulate the unexpected higher levels of OH in isoprene rich environments. This could become an especially serious issue as Hofzumahaus et al. (2009) reported significantly higher (~ 2.6 times at noon) than expected OH levels in the Pearl River Delta region in China. Therefore, the current assessments based on the conventional OH photochemistry could

146 significantly misdiagnose regional air-quality status and mislead policy implementation
147 to reduce photochemical air pollution in the East Asian region. Furthermore, as the
148 importance of BVOC in regional air-quality issues in ozone and SOA formation has been
149 also highlighted in Europe and North America, the uncertainty in isoprene
150 photochemistry has significant implications in urban and suburban air quality in general
151 (Zhang et al., 2008a;Sartelet et al., 2012).

152 We present atmospheric observations of NO_X, CO, VOCs, ozone, and HONO in
153 the Taehwa Research Forest (TRF) in the Seoul Metropolitan Area (SMA), South Korea.
154 We use observed data from June, 2013 to conduct observationally constrained box model
155 (University of Washington Chemical Box Model; UWCM) calculations to estimate OH,
156 HO_2 and RO_2 concentrations with different sets of observational parameters. We discuss
157 current uncertainty in OH-isoprene photochemistry with perspectives of constraining
158 photochemical ozone production and OVOCs precursors of secondary organic aerosols.
159

160 2. **Methods**

161 The Taehwa Research Forest (TRF) is located ~ 35 km from the center of Seoul,
162 South Korea. The TRF is located at the southeastern edge of the Seoul metropolitan Area
163 (SMA, population of ~ 23 million). TRF has a sampling tower located in the middle of a
164 coniferous tree plantation (200 m by 200 m) with the canopy height of 18 m (*Pinus*
165 *koraiensis*) surrounded by a deciduous forest mostly composed by oak. The TRF
166 instrumentation has previously been described by Kim et al. (2013d) along with the
167 previous trace gas observational results. Therefore, just brief descriptions of analytical
168 techniques are given in this paper.

169

170 **2.1. CO, NO_X, SO_2, ozone, VOCs, and meteorological parameters**

171 Thermo Fisher Scientific Enhanced Trace Level Gas Analyzers are used for CO,
172 NO_X, SO_2, and ozone observations as summarized Table 1. VOC observations are
173 conducted by a High-Sensitivity Proton Transfer Reaction-Mass Spectrometer (PTR-MS,
174 Ionicon GmbH). The atmospheric application of this technique is thoroughly reviewed by
175 de Gouw and Warneke (2007). In addition, the instrument suite at TRF is thoroughly
176 described in (Kim et al., 2013d). PTR-MS can quantify atmospheric VOCs that have
177 higher proton affinity than the proton affinity of H_2O (691 kJ mol^{-1}). Most alkanes have
178 lower proton affinity than water but alkene, aromatic and some OVOCs have higher
179 proton affinity and are suitable for quantification using PTR-MS (Blake et al., 2009).
180 These compounds are more reactive than alkane compounds so PTR-MS has capability to
181 observe reactive atmospheric compounds. The TRF PTR-MS system was set to measure
182 acetaldehyde, acetone, acetic acid, isoprene, methylvinylketone (MVK) + methacrolein
183 (MACR), MEK, benzene, xylene (*p*, *m*, and *o*), and monoterpenes (MT). Each compound
184 was set to be monitored for 1 second each resulting in a sample cycle of 15 seconds.
185 Lower detection limits for the observed VOCs are estimated to be 20 ppt for a 5 second
186 integration with sensitivity of 70 counts ppb^{-1} (2 σ). The uncertainty is estimated as 12 %
187 (2 σ) for the same integration time. Meteorological parameters such as temperature and
188 humidity are monitored by LSI LASTEM Meteorological Sensors. All the presented data
189 is from the 15 m (the canopy height is 18 m) sampling line and meteorological sensors
190 collocated at this height too.

PTR-MS with a quadrupole mass filter has an intrinsic limitation that isobaric compounds are all collectively quantified with the same channel (m/z) with a resolution of unit mass. This limitation particularly becomes an issue for investigating the roles of different isomers of MT and sesquiterpenes (SQTs) in photochemistry. For this reason, we also occasionally collect sorbent cartridge samples to analyze MT and SQT speciation in both ambient air and branch enclosure emissions near the sampling tower. As described in (Kim et al., 2013d), Tenax GR and Carbotrap 5TD packed sorbent cartridges (Markes Int, Llanstrisant, UK) were used for sampling. The sampled cartridges were shipped to National Center for Atmospheric Research (NCAR), Boulder CO, USA for gas chromatography-mass spectrometer (GC-MS) analysis. An Agilent 7890 GC/5975 C Electron Impact Mass Spectrometer (GC-MS/FID) in conjunction with a MARKES Unity1/Ultra thermal desorption system optimized for terpenoid analysis quantifies speciated MT and SQT in the sorbent samples. Cartridge samples are both collected from ambient and branch enclosure air. Ambient samples were collected in the mid-day to early afternoon with a volume of 6 L. Ozone in the ambient air was removed using a Na_2SO_3 filter. Branch enclosure samples were also collected, mostly in the mid-day time frame, with a volume of 1 L without an ozone filter as zero air was introduced to the branch enclosure. To explore the diurnal differences in BVOC emissions, some branch enclosure sampling was conducted continuously for three consecutive days in mid June of 2013. We present these analytical results from GC-MS analysis limited to the qualification purpose to examine MT and SQT speciation.

2.2 HONO quantification

HONO was measured with an ion chromatography (IC) coupled with diffusion scrubber. Air was introduced to diffusion scrubber (Lab solutions Inc., IL, USA) through a 2 m PFA tubing (1/4" i.d.) at 1.5 L m^{-1} using a filtered orifice restrictor (F-950, air logic, WI, USA). Air flowing through diffusion scrubber interfaced with deionized water, into which HONO was extracted. 50 μL of solution was injected into the IC system through a PEEK loop (Rheodyne, WA, USA) and 6-way valve (EV750-100, Rheodyne, WA, USA). Eluent was a mixture of Na_2CO_3 and $NaHCO_3$, which was pumped by a HPLC pump (DX-100, Dionex, CA, USA) into a guard column (Ionpax® AG 14, 4x50mm, Dionex, CA, USA) and then analytical column (Ionpax® AS 14, 4x250mm, Dionex, CA, USA). The column effluent passed through a suppressor (ASRS 300, Dionex, CA, USA) and HONO was detected as nitrite ion in conductivity detector (550, Alltech, IL, USA). The entire measurement processes of sampling, chemical analysis, and data acquisition were controlled by a digital timer and data acquisition software (DSchrom-n, DS science, Korea), by which we obtained two measurements every hour. The system was calibrated using a NO_2^- standard solution (Kanto chemical Co., Inc., Tokyo, Japan) whenever reagents were replaced. The detection limit was 0.15 ppb estimated from 3σ of the lowest working standard. Specific analytical characteristics are described in Simon and Dasgupta (1995) and Takeuchi et al. (2004).

2.3 UWCM box model

UWCM 2.1 is an open source box model coded by MATLAB (MathWorks®). The model platform can be downloaded from a website (http://sites.google.com/site/wolfegm/code-archive). The box model is embedded its own

237 HO_X ($OH+RO_2$)-RO_X (peroxyradical and alkoxy radical)-NO_X coupling chemical
238 mechanism. UWCM utilizes Master Chemical Mechanism version 3.2 (MCM 3.2)
239 (Jenkins et al., 1997; Saunders et al., 2003) for near-explicit VOC photo-oxidation
240 schemes. A more detailed model description can be found in Wolfe and Thornton (2011).
241 To minimize uncertainty from the parameterizations of transport and emission, we
242 constrained relatively long-lived trace gases presented in Figure 1. This box modeling
243 technique has been commonly used for examination of OH levels that can be justified by
244 the short chemical lifetime of OH (Kim et al., 2014;Kim et al., 2013c;Mao et al.,
245 2012;Mao et al., 2010). Recently developed isoprene photo-oxidation mechanisms
246 shown in Archibald et al. (2010) are also incorporated in the model. In addition, Kim et al.
247 (2013c) and Wolfe et al. (2013) applied the model in the identical fashion as used for this
248 study to probe radical distributions using comprehensive observational datasets. This
249 study used the UWCM to simulate the diurnal variations of radical pool ($OH+HO_2+RO_2$)
250 distributions as observational parameters such as CO, NO_X, ozone, and VOCs are
251 constrained. To fully account for roles of OVOCs in the box model as radical sources, we
252 simulated three consecutive days and presented diurnal variations from the third day. The
253 specific parameters, constrained by observations are described in section 2.1 and 2.2.
254
255 **3. Results**
256 **3.1. Observational Results**
257 Diurnal averages of observed trace gases (June 1st 2012 to June 6th 2012) are
258 shown in Figure 1. The TRF observatory is in continuous operation and we choose this
259 six day period because a regional high-pressure system caused a stagnant air pollution

event in this period. In the center of Seoul (the real- time data available at http://www.airkorea.or.kr), carbon monoxide was observed in the similar levels during the focused period (June 1st to June 6th, 2012). On the other hand, the NO_2 level observed in central Seoul was much higher (20-50 ppb) compared with observed levels at TRF. The reason can be attributed to differences between the chemical lifetime of CO (~a month) and NO_2 (~a few hours to a day). The observations clearly indicate that the TRF is not directly influenced by fresh SMA pollution plumes although the TRF is very close to the center of Seoul (30 km away from the city center) as a regional modeling study shows most of CO and NO_X sources are located in the city center (Ryu et al., 2013). Similar observations were also reported for other East Asian megacities such as Beijing (Ma et al., 2012), where ~ 30 ppb and ~ 15 ppb of NO_2 were observed at noon in the urban and the adjacent rural sites, respectively. In contrast, there were no noticeable differences in CO levels between the urban and rural sites (~ 1-2 ppm). The observed CO, NO_X and SO_2 levels in TRF were much lower than those observed in the suburban regions of Chinese megacities such as Beijing (Ma et al., 2012), Shanghai (Tie et al., 2013), and the Pearl River Delta Region (Lu et al., 2012) and similar with the observed levels in Tokyo, Japan (Yoshino et al., 2012).

Previous VOC observations in the SMA consistently have shown that toluene is the dominant anthropogenic VOC followed by other aromatic compounds such as xylene and benzene (Kim et al., 2012;Na and Kim, 2001). Na and Kim (2001) reported high concentrations of propane from house hold fuel use. However, recent observation results from the photochemical pollution observational network managed by National Institute of Environmental Research (NIER) of South Korea in the SMA clearly indicate that propane

283 levels have declined and are now much lower than the levels previously observed (NIER,
284 2010). This is probably caused by the implementation of a policy changing household
285 fuel sources from propane to methane. Kim et al. (2012) presented detailed aromatic
286 VOC distributions in the SMA from four different urban observational sites. In average,
287 toluene concentrations were observed ~ 7 times higher than the observed levels of xylene
288 and benzene. At the TRF, a similar anthropogenic VOC speciation distribution was
289 observed as shown in Figure 1. The observed toluene and MEK (methyl ethyl ketone)
290 mixing-ratios were much higher than benzene and xylene. MEK is detected in m/z of 73^+
291 by PTR-MS. Although methyl glyoxal, an atmospheric VOC oxidation product, is also
292 detected on the same mass, we assumed that 73^+ of m/z signals are mostly from MEK, an
293 anthropogenic VOC, since the temporal variation follows that of anthropogenic VOC
294 such as toluene and xylene. In addition, atmospheric lifetime of methyl glyoxal is much
295 shorter than MEK.
296 As the observation facility is located in the middle of a pine tree plantation (*Pinus*
297 *koraiensis*), monoterpenes (MT) are consistently observed. The temporal variation of
298 monoterpenes is affected by the planetary boundary layer evolution with a pattern of
299 higher MT levels during night than those of mid-day as has been often reported in other
300 forest environments (Bryan et al., 2012;Kim et al., 2010) This can be explained by
301 interplays between boundary layer evolution and temperature dependent MT emission. It
302 should also be noted that the continuous branch enclosure BVOC emission observations
303 indicate that the daily maxima of MT and SQT emissions were observed in the midday
304 (between noon to 2 pm in the local time). The observed MT and SQT speciation
305 information in the midday is summarized in Table 2. Table 2a summarizes branch

306 enclosure sample analysis results and ambient sample analysis results are summarized in
307 Table 2b. In general, observed MT and SQT in the ambient air are consistent with
308 previously observed distributions (Kim et al., 2013d). α-pinene and β-pinene were the
309 dominant monoterpene and longifolene was the only detected SQT species. In contrast,
310 the branch enclosure observation results, reflecting BVOC emission, indicate high
311 emission of very reactive MT and SQT species such as β-myrcene, α-caryophyllene, and
312 β-caryophyllene. The fast oxidation of these highly reactive terpenoid species is expected
313 to limit the atmospheric presence of the compounds. Therefore, photochemical oxidation
314 processes of these compounds may have been neglected. Investigating emissions and
315 photochemistry of these reactive terpenoid compounds can constrain potential missing
316 OH reactivity and SOA production from highly oxidized reaction products.
317 Isoprene is produced from carbon recently fixed through photosynthesis resulting
318 in higher emissions and atmospheric concentrations during the daytime. The temporal
319 variation shown in Figure 1 reveals an isoprene concentration maximum between 17:00
320 to 20:00. In addition, the ratios of MVK+MACR, major isoprene oxidation products and
321 isoprene at this period, are significantly lower than those of late morning to early
322 afternoon. The enhanced isoprene levels in the late afternoon or early evening have been
323 also reported in previous studies (Apel et al., 2002;Bryan et al., 2012). The branch
324 enclosure observations demonstrate that isoprene is not emitted from the pine plantation
325 but rather transported from surrounding broadleaf forests as right outside of the pine
326 plantation (200 m × 200 m) is a forested area dominated by oak trees. Oak comprises 85 %
327 of broadleaf trees in South Korea (Lim et al., 2011). Lim et al. (2011) quantified isoprene
328 emission rates for five representative oak species in South Korea and report a wide

329 emission range from oaks that are negligible isoprene emitters (<0.004 μgC dw^{-1} h^{-1};
330 standard emission rates) to others with very high isoprene emission rates of 130 μgC dw^{-1}
331 h^{-1}.

332 Contributions from each trace gas species towards ambient OH reactivity are
333 shown in Figure 2. This is calculated as the product of the observed species concentration
334 and its rate constant for reaction with OH. Observed OH reactivity from VOCs are much
335 higher than from other trace gases such as CO, NOx, SO_2, and ozone. Among the
336 observed VOC species, BVOCs such as isoprene, α-pinene and β-pinene accounted for
337 significantly higher OH reactivity in comparison with the observed AVOCs such as
338 toluene, benzene, xylene and MEK. Isoprene accounts the highest OH reactivity
339 especially during the daytime. This analysis is consistent with reports from other
340 suburban observations from East Asian megacities such as Beijing (Ran et al., 2011), the
341 PRD region, China (Lou et al., 2010), and the Kinki region Japan (Bao et al., 2010).

342 HONO levels up to 1 ppb were observed in the early morning and were
343 consistently higher than 0.5 ppb during the daytime. These observed levels are
344 substantially higher than reported observations from forest environments in North
345 America (Ren et al., 2011;Zhou et al., 2011), where NO_X (~ 1 ppb) is substantially lower
346 than the level observed at TRF. Ren et al. (2011) reported 30 – 60 ppt of HONO at the
347 Blodgett Forest Research Station in the western foothills of the Sierra Nevada Mountains
348 in the late summer of 2007. Zhou et al. (2011) also reported the similar levels of HONO
349 (below 100 ppt) from the PROPHET forest, a mixed hardwood forest in northern
350 Michigan (Pellston, MI). However, significantly higher HONO levels (~ 200 ppt to ~ 2
351 ppb) were reported by Li et al. (2012) from a rural observational site in the Pearl River

352 Delta region near Guangzhou, where comparable NO_2 levels with TRF were observed.
353 The high HONO levels (a few hundred ppt) especially during the daytime have been
354 consistently reported near Eastern Asian megacities such as Beijing (Li et al., 2012),
355 Shanghai (Hao et al., 2006), and Seoul (Song et al., 2009). Still these are limited datasets
356 and further comprehensive analysis, especially more extensive observation is required.
357 However, two recently proposed HONO production mechanisms may be able to explain
358 the higher levels in the Eastern Asian megacity region. One is HONO production from
359 NO_2 photo-excitation (Wong et al., 2012) as the region usually has high NO_2
360 concentrations and the other is HONO emission from soil bacteria (Oswald et al., 2013).
361 Oswald et al. (2013) found differences as much as two orders of magnitude in HONO
362 emissions from soil samples from different environments (e.g. pH and nutrient contents).
363 In addition, as most of observations in the East Asia regions were conducted with ion
364 chromatography based methods, more direct HONO quantification techniques such as a
365 chemical ionization mass spectrometry technique (Roberts et al., 2010) need to be used to
366 characterize any potential interferences such a high NO_X environment (e.g. N_2O_5).
367
368 **3.2 HO_X Model calculations with different isoprene photo-oxidation scenarios and**
369 **the roles of unconstrained HONO sources in HO_X model evaluations.**
370 The presented observational results are used to constrain the UWCM box model.
371 We evaluate uncertainties in the tropospheric oxidation capacity and how it affects our
372 ability to constrain ozone and OVOCs production. The observational results clearly
373 indicate that isoprene is the most dominant OH sink among the observed VOCs. In
374 addition, NO concentrations were higher in the 600 to 800 ppt range in the morning. On

375 the other hand, afternoon levels were substantially lower in the 50 to 100 ppt range. The
376 environment provides a unique opportunity to examine implications of isoprene
377 photochemistry in various NO conditions.
378 We conducted model simulation under six different scenarios. Each scenario is
379 described in Table 3. The quantitative assessments of the impacts to radical
380 concentrations (OH, HO_2, and RO_2) from unknown HONO sources are evaluated by
381 examining the model outcomes of the scenarios with and without observed HONO. To
382 evaluate the impacts of hydroperoxy-methyl-butenal (HPALD) photolysis and isoprene
383 peroxy radical recycling in the radical pool, each chemical mechanism is selectively
384 constrained by different scenarios. For HPALD chemistry, we adapted two different
385 HPALD formation rate constants published by Peeters and Muller (2010) and Crounse et
386 al. (2011). The formation rates from Peeters and Muller (2010) is about 40 times faster
387 than those from Crounse et al. (2011) in 298 K. Finally, we applied the OH yield of 2.6
388 from isoprene peroxy radical and HO_2 reactions for the evaluation (Wolfe et al., 2011).
389 Although, Liu et al. (2013) demonstrated significantly lower OH recycling contributions
390 from HO_2 + isoprene peroxy radical reactions than those argued by Wolfe et al. (2011) by
391 interpreting chamber experiment results, the high recycling rate from Wolfe et al. (2011)
392 is applied in the model calculations to explore upper limit of uncertainty in radical
393 estimations.
394 Modeled OH, HO_2, and RO_2 from the six different model scenarios are shown in
395 Figure 3. A summary of averaged OH, HO_2, and RO_2 concentrations in the morning
396 (08:00 – 11:00) and the afternoon (13:00 – 16:00) from each simulation is shown in
397 Table 4. With respect to the base run results (Scenario I), Scenario III with the lower

HPALD formation rate does not cause noticeable differences in radical concentrations. Adapting higher HPALD formation rates (Scenario II) cause significant differences in radical distribution especially in RO_2. This difference is likely caused by the fact that significant isoprene peroxy radical is converted to HPALD. The higher levels of discrepancy is found in RO_2 between Scenario I and Scenario II in the afternoon when low NO concentrations are observed, which efficiently facilitates HPALD formation. Adding HO_2 + isoprene peroxy radical reactions as OH recycling processes (Scenario IV and V) results in significant enhancements in OH and HO_2 with respect to the base run (Scenario I). RO_2 concentrations are calculated in significantly different levels between Scenario IV and V. This can be again accounted by the applications of different HPALD formation rates in the two different model scenarios. The higher level of OH from the additional recycling process causes substantially higher RO_2 formation rates than those from the scenarios without the additional recycling process. The faster HPALD formation in Scenario IV appeared to cause faster loss of RO_2 resulting in low RO_2 concentrations.

Striking differences can be found in the model simulation results with or without constraining observed HONO as shown in Figure 3. Model calculation results from Scenario VI indicate significantly smaller OH, HO_2, and RO_2 concentrations than the concentrations calculated from the counter part (Scenario IV), which contains identical constraints and isoprene photochemistry except constraining observed HONO. Again, this clearly indicates that more thorough evaluations of the impacts of HONO on air quality are needed to precisely constrain photochemical processes in the region along with evaluations of the currently available analytical techniques as argued in section 3.1.

3.3 Implications of uncertainty in HO_X model calculations in assessing photochemical ozone and OVOC production.

Two competing chemical reactions (R3 vs. R4,5,6) determine radical distribution regimes.

$$RO_2 + NO \rightarrow RO + NO_2 \quad (R3)$$

$$RO_2 + HO_2 \rightarrow ROOH + O_2 \quad (R4)$$

$$RO_2 + RO_2 \rightarrow ROOR + O_2 \quad (R5)$$

$$HO_2 + HO_2 \rightarrow H_2O_2 + O_2 \quad (R6)$$

When the rate of R3 gets much faster than the sum of reaction rates of R4, R5, and R6 then radical recycling processes become more efficient than radical destruction processes. In this radical recycling regime, OH, a universal tropospheric oxidant, is well buffered to maintain the elevated OH levels. On the other hand, the radical destruction regime can be defined when the radical recycling rates (R3) are slower than the radical destruction reaction rates (R4+R5+R6). Although some recent findings (e.g. Lelieveld et al. (2008)) suggest that we may need to reconsider R4 as a radical recycling process rather than a radical destruction process, in this study, we follow the conventional classification of radical chemistry regimes. The temporal variations of radical-radical reaction rates from the model simulation scenarios are shown in Figure 4. In general, the radical reaction rates are elevated as much as twice once observed HONO is constrained in the model calculations (e.g. Scenario VI). This is because unaccounted HONO in the model calculations cause significant underestimations in the radical pool ($OH+HO_2+RO_2$)

size with respect to the constrained HONO scenarios as shown in Figure 4. In addition, as we include recently developed isoprene radical chemistry, the RO_2+HO_2 reaction rates, known for a radical destruction pathway becomes more faster. This becomes more obvious in the afternoon when NO concentration becomes lower. The RO_2 + HO_2 reaction rates get higher than those of RO_2 + NO in the afternoon for the Scenario IV and V. This is surprising, as the radical destruction regime is usually associated with low NO_X conditions. Suburban regions of megacities including the TRF in general show high NO_X conditions. However, radical recycling rates are determined by concentrations of NO. The fraction of NO in the NO_X pool is determined by competing reactions between NO_2 photolysis and oxidation reactions of NO by ozone, HO_2, and RO_2 radicals. Once we assume the pseudo-steady state of NO, then NO in NO_X pool can be expressed as

$$[NO] = J_{NO2}[NO_2]/(k_{NO+O3}[O_3] + k_{NO+HO2}[HO_2] + k_{NO+RO2}[RO_2]) \quad (R7)$$

This mathematical expression clearly shows that NO levels are dependent on NO_X mostly composed of NO_2. At the same time, the fraction of NO in NO_X is anti-correlated with ozone, HO_2, and RO_2 concentrations. Therefore, the size of the radical pool composed of HO_2 and RO_2 is relevant for determining the fractions of NO in given NO_X levels. High HO_2 and RO_2 are likely observed in high VOC regions such as forested areas. This could cause a smaller fraction of NO in the given NO_X pool so radical recycling gets relatively weaker compared with radical destruction reaction pathways. More quantitative approaches are required to categorize radical reaction pathways rather than qualitative categorization such as high or low NO_X regimes.

Conventionally, efficient ozone production can be achieved by the balance between nitric acid production rates (P_{HNO3}, $OH + NO_2$) and peroxide production rates (P_{ROOH}, HO_2+RO_2 or P_{H2O2} HO_2+HO_2) (Sillman and He, 2002). The imbalance will cause ozone production sensitivity towards either NOx or VOCs. A comprehensive photochemical model analysis (Tonnesen and Dennis, 2000a, b) demonstrated that in a wider range of ozone concentrations, the VOC and NOx limited regimes can be determined by the ratios of P_{H2O2} and P_{HNO3}. The ratio range (P_{H2O2}/P_{HNO3}) of 0.35 is regarded as the border range. In the VOC limited regime ($P_{H2O2}/P_{HNO3} < 0.35$), ozone production is expected to decrease with increasing NO_X and increase with increasing VOCs. In the NO_X limited regime ($P_{H2O2}/P_{HNO3} > 0.35$), ozone production gets efficient with increasing NO_X and is insensitive to changes in VOCs (Sillman and He, 2002). This categorization has guided policy-making processes whether NO_X or VOC controls will be more effective in ozone reduction. A series of modeling studies have been conducted to characterize ozone production regimes in the suburban regions of East Asian megacities and have consistently concluded that the role of isoprene is important in ozone production. However, most of these studies have concluded that East Asian megacity regions are mostly in the VOC limited regime (Tseng et al., 2009;Zhang et al., 2008b;Lim et al., 2011;Cheng et al., 2010;Shao et al., 2009a;Shao et al., 2009b;Xing et al., 2011). Recently, however, a modeling study by Li et al. (2013) in the Pearl River Delta region in China demonstrated the time dependence of ozone production regimes. Specifically, with high NOx emissions in the morning, the regional ozone production regime is categorized as VOC limited. In contrast, in the afternoon when the highest ozone concentrations are observed, a NOx limited regime is often found. The obvious

490 issue to be addressed is that all of the above studies neglected how the uncertainty in
491 hydroxyl radical chemistry would affect the ozone production regime. Moreover, HONO
492 has been rarely constrained by observations in the previous modeling studies. Figure 5
493 shows the temporal variations of P_{H2O2}/P_{HNO3} from the all six different model scenarios.
494 The VOC limited ozone formation regime was observed regardless of the HO_X
495 simulation scenarios. Differences among the scenarios are not noticeable in the morning
496 when NO is high but noticeable differences can be found in the afternoon which may
497 cause uncertainty in assessing the optimal level of NO_X and VOC emission
498 controls from a policy perspective. In general, the model calculation results with
499 faster HPALD formation rates indicate higher $P(H_2O_2)/P(HNO_3)$ in the afternoon. This
500 analysis indicates that it is difficult to determine an effective policy implementation for
501 NO_X or VOC controls to achieve ozone abatement around Asian megaticities where
502 isoprene is a significant OH sink without accurate understanding of radical isoprene
503 interactions (e.g. Kim et al. (2013b)).
504 Another unresolved uncertainty in understanding tropospheric OH is its chemical
505 loss rates. The limited observations of OH reactivity in BVOC dominant environments
506 show consistent unaccounted OH chemical loss with observational datasets (Di Carlo et
507 al., 2004;Edwards et al., 2013;Kim et al., 2011;Lou et al., 2010;Nolscher et al.,
508 2012;Nakashima et al., 2014;Sinha et al., 2010). Two different processes are speculated
509 to cause unaccounted OH loss known as missing OH reactivity: 1) primary emissions of
510 unmeasured or unknown compounds and 2) oxidation products of well-known BVOCs
511 especially isoprene. Most studies conducted in coniferous forests where monoterpenes
512 are dominant primary BVOC emissions have concluded that unmeasured or unknown

513 primary BVOC emissions caused missing OH reactivity (Sinha et al., 2010;Nakashima et
514 al., 2014). On the other hand, studies conducted in isoprene dominant environments in
515 mostly broadleaf or mixed forests have concluded that the main cause of missing OH
516 reactivity is the oxidation products of isoprene (Edwards et al., 2013;Kim et al., 2011).
517 Edwards et al. (2013) presented a thorough analysis on potential impacts of isoprene
518 oxidation products that are not routinely constrained by observations. The authors found
519 significant contributions from secondary oxidation products such as multi-functional
520 oxygenated compounds.
521 Figure 6a shows the temporal variations of total OH reactivity calculated from
522 five different model scenarios (I through V). The highest and the lowest OH reactivity
523 levels were predicted from model calculations of Scenario V and Scenario II, respectively.
524 This observation is directly correlated with calculated RO_2 levels as the lowest and
525 highest RO_2 levels were calculated from Scenario II and Scenario V, respectively. Since
526 VOC precursors and trace gases were all constrained by observations in the model
527 calculations, the differences in model calculated OH reactivity should be mainly caused
528 by the oxidation products of VOCs. This can be confirmed by the comparisons of model
529 calculated formaldehyde concentrations from Scenario II and V as formaldehyde is a
530 dominant oxidation product of isoprene (Figure 6b). The differences in formaldehyde
531 levels suggest differences in OH reactivity levels from OVOCs in each model simulation.
532 In summary, uncertainty in radical distributions especially RO_2 levels is directly
533 propagated into uncertainty in OVOC formation.
534 These calculated results provide an upper limit of potential contributions from the
535 oxidation products of the constrained VOC precursors considering that the box-model

536 does not consider dry-deposition processes as Karl et al. (2010) and Edwards et al. (2013)
537 suggested that there is significant uncertainty associated with the parameterizations of dry
538 deposition especially OVOCs. Still, this analysis suggests that significant missing OH
539 reactivity (~ up to factor of two to three) can be found without constraining OVOCs.
540 OVOCs, especially multi-functional highly oxidized compounds are precursors for
541 secondary organic aerosols (VOCs). Therefore, uncertainty surrounding missing OH
542 reactivity significantly undermines our ability to constrain SOA formation and aerosol
543 growth.
544

545 ## 4. Summary and conclusions

546 We presented trace gas observation results from the TRF near the center of
547 Seoul, South Korea. The dataset provides important constraints to evaluate the HO_X
548 pool at the site where both anthropogenic and biogenic influences become important
549 factors in determining oxidation capacity. Although the site is in the vicinity of a
550 megacity with 25 million people, isoprene accounted for most of the OH loss from
551 observed atmospheric hydrocarbon species during the 6-day focus period in early June
552 2012 during a regional pollution episode. In addition, observed NO_X levels were
553 substantially lower than observed values in the center of the SMA. These observations
554 indicate that impacts of megacity pollution on suburban BVOC photochemistry can be
555 observed at the TRF.
556 Six different model scenarios are employed to investigate the radical (OH, HO_2,
557 and RO_2) distributions using the UWCM box-model. The observed trace gas data were
558 constrained and the photochemical mechanisms (MCM 3.2) of seven VOC species with

559 high levels at the TRF were integrated. The uncertainty in isoprene peroxy radical
560 chemistry results in a wider range of OH, HO_2, and RO_2 distributions. Unconstrained
561 HONO sources also cause a quite high level of underestimation in a radical pool
562 ($OH+HO_2+RO_2$). OH simulation from the different model scenarios indicates much
563 larger discrepancies (up to three times) than simulations for HO_2 and RO_2 (up to twofold).
564 OH is simulated in much higher levels with the consideration of an additional OH
565 recycling channel from isoprene peroxy radical + HO_2 reactions and fast HPALD
566 formation chemistry Peeters and Muller (2010). On the other hand, the RO_2 simulations
567 result in lower levels as HPALD formation depletes the RO_2 pool, which mostly
568 composed by isoprene peroxy radicals. These results suggest that HO_2 and RO_2
569 observations can provide pivotal information about radical recycling and isoprene peroxy
570 radical chemistry (Kim et al., 2013c;Wolfe et al., 2013). More studies on characterizing
571 existing techniques to quantify HO_2 (Fuchs et al., 2011) and developing new techniques
572 (Horstjann et al., 2013) are needed. In addition, the simulations with recently developed
573 isoprene photo-oxidation chemistry show that radical termination processes (e.g.
574 peroxide formation) get more efficient than radical recycling processes in the afternoon.
575 This may come as a surprise as in general we expect the high NO_X conditions in the
576 suburban regions of a megacity to have effective radical recycling. However, the critical
577 factor determining competing reaction channels of recycling and peroxide formation is
578 NO concentrations. Ratios of NO to NO_2 are not only correlated with NO_2 concentrations
579 and photolysis constants but also anti-correlated with RO_2, HO_2 and ozone concentrations
580 and relevant kinetic constants as shown in (R7). Therefore, a semi-quantitative term such

as the high 'NO_X' regime is not a proper term to define radical recycle regimes especially in high radical environments (e.g. HO_2 and RO_2) such as forest environments.

These uncertainties in estimating the radical pool size and distribution directly affect our ability for constraining photochemical ozone and OVOC production. The non-linear response of ozone production to NO_X and VOC abundances are determined by OH, HO_2, RO_2 and NO_2 concentrations. Regardless of which model calculation scenario we adapt, the TRF photochemical state appears to be a VOC limited ozone production regime. However, morning and afternoon show a very strong contrast. The morning conditions indicate a stronger degree of VOC limitation. In addition, a noticeable range of VOC sensitivity was calculated from the six different model scenarios, especially in the afternoon. These analysis results, therefore, suggest that an accurate scientific understanding of isoprene-OH interactions should form the basis for an effective policy implementation to reduce photochemical pollution in the suburbs of Seoul and similar East Asian megacities. In addition, OVOC production is predicted to significantly vary depending on the model simulation scenarios. The fate of these OVOCs is uncertain and can include deposition, photolysis, or condensation. Our limited understanding of OVOCs contributes substantially to the overall uncertainty in radical photochemistry and should be addressed by studies that quantify the processes controlling OVOC production and loss.

Acknowledgements

This research is financially supported by the National Institute of Environmental Research of South Korea. The authors appreciate logistical support from the research and supporting staff at Taehwa Research Forest operated by Seoul National University.

References

Apel, E. C., Riemer, D. D., Hills, A., Baugh, W., Orlando, J., Faloona, I., Tan, D., Brune, W., Lamb, B., Westberg, H., Carroll, M. A., Thornberry, T., and Geron, C. D.: Measurement and interpretation of isoprene fluxes and isoprene, methacrolein, and methyl vinyl ketone mixing ratios at the PROPHET site during the 1998 Intensive, J Geophys Res-Atmos, 107, Artn 4034 Doi 10.1029/2000jd000225, 2002.

Archibald, A. T., Jenkin, M. E., and Shallcross, D. E.: An isoprene mechanism intercomparison, Atmos Environ, 44, 5356-5364, Doi 10.1016/J.Atmosenv.2009.09.016, 2010.

Arneth, A., Schurgers, G., Lathiere, J., Duhl, T., Beerling, D. J., Hewitt, C. N., Martin, M., and Guenther, A.: Global terrestrial isoprene emission models: sensitivity to variability in climate and vegetation, Atmos Chem Phys, 11, 8037-8052, Doi 10.5194/Acp-11-8037-2011, 2011.

Bao, H., Shrestha, K. L., Kondo, A., Kaga, A., and Inoue, Y.: Modeling the influence of biogenic volatile organic compound emissions on ozone concentration during summer season in the Kinki region of Japan, Atmos Environ, 44, 421-431, Doi 10.1016/J.Atmosenv.2009.10.021, 2010.

Barket, D. J., Hurst, J. M., Couch, T. L., Colorado, A., Shepson, P. B., Riemer, D. D., Hills, A. J., Apel, E. C., Hafer, R., Lamb, B. K., Westberg, H. H., Farmer, C. T., Stabenau, E. R., and Zika, R. G.: Intercomparison of automated methodologies for determination of ambient isoprene during the PROPHET 1998 summer campaign, J Geophys Res-Atmos, 106, 24301-24313, Doi 10.1029/2000jd900562, 2001.

Blake, R. S., Monks, P. S., and Ellis, A. M.: Proton-Transfer Reaction Mass Spectrometry, Chem Rev, 109, 861-896, 2009.

Bryan, A. M., Bertman, S. B., Carroll, M. A., Dusanter, S., Edwards, G. D., Forkel, R., Griffith, S., Guenther, A. B., Hansen, R. F., Helmig, D., Jobson, B. T., Keutsch, F. N., Lefer, B. L., Pressley, S. N., Shepson, P. B., Stevens, P. S., and Steiner, A. L.: In-canopy gas-phase chemistry during CABINEX 2009: sensitivity of a 1-D canopy model to vertical mixing and isoprene chemistry, Atmos Chem Phys, 12, 8829-8849, Doi 10.5194/Acp-12-8829-2012, 2012.

Chameides, W. L., Lindsay, R. W., Richardson, J., and Kiang, C. S.: The Role of Biogenic Hydrocarbons in Urban Photochemical Smog - Atlanta as a Case-Study, Science, 241, 1473-1475, 1988.

Chang, C. C., Wang, J. L., Leung, S.-C. C., Chang, C. Y., Lee, P.-J., Chew, C., Liao, W.-N., and Ou-Yang, C.-F.: Seosonal characteristics of biogenic and anthropogenic isoprene in tropical-subtropical urban environments, Atmos Environ, 99, 298-308, 2014.

644 Cheng, H. R., Guo, H., Saunders, S. M., Lam, S. H. M., Jiang, F., Wang, X. M., Simpson, I.
645 J., Blake, D. R., Louie, P. K. K., and Wang, T. J.: Assessing photochemical ozone
646 formation in the Pearl River Delta with a photochemical trajectory model, Atmos
647 Environ, 44, 4199-4208, Doi 10.1016/J.Atmosenv.2010.07.019, 2010.
648 Crounse, J. D., Paulot, F., Kjaergaard, H. G., and Wennberg, P. O.: Peroxy radical
649 isomerization in the oxidation of isoprene, Phys Chem Chem Phys, 13, 13607-13613,
650 Doi 10.1039/C1cp21330j, 2011.
651 de Gouw, J., and Warneke, C.: Measurements of volatile organic compounds in the
652 earths atmosphere using proton-transfer-reaction mass spectrometry, Mass
653 Spectrom Rev, 26, 223-257, 2007.
654 Di Carlo, P., Brune, W. H., Martinez, M., Harder, H., Lesher, R., Ren, X. R., Thornberry,
655 T., Carroll, M. A., Young, V., Shepson, P. B., Riemer, D., Apel, E., and Campbell, C.:
656 Missing OH reactivity in a forest: Evidence for unknown reactive biogenic VOCs,
657 Science, 304, 722-725, Doi 10.1126/Science.1094392, 2004.
658 Edwards, P. M., Evans, M. J., Furneaux, K. L., Hopkins, J., Ingham, T., Jones, C., Lee, J.
659 D., Lewis, A. C., Moller, S. J., Stone, D., Whalley, L. K., and Heard, D. E.: OH reactivity in
660 a South East Asian tropical rainforest during the Oxidant and Particle Photochemical
661 Processes (OP3) project, Atmos Chem Phys, 13, 9497-9514, Doi 10.5194/Acp-13-
662 9497-2013, 2013.
663 Fuchs, H., Bohn, B., Hofzumahaus, A., Holland, F., Lu, K. D., Nehr, S., Rohrer, F., and
664 Wahner, A.: Detection of HO2 by laser-induced fluorescence: calibration and
665 interferences from RO2 radicals, Atmos Meas Tech, 4, 1209-1225, Doi 10.5194/Amt-
666 4-1209-2011, 2011.
667 Guenther, A.: Biological and chemical diversity of biogenic volatile organic emissions
668 into the atmosphere, Atmospheric Sciences, 2013, ArticleID 786290, 2013.
669 Hao, N., Zhou, B., Chen, D., and Chen, L. M.: Observations of nitrous acid and its
670 relative humidity dependence in Shanghai, J Environ Sci-China, 18, 910-915, Doi
671 10.1016/S1001-0742(06)60013-2, 2006.
672 Hofzumahaus, A., Rohrer, F., Lu, K. D., Bohn, B., Brauers, T., Chang, C. C., Fuchs, H.,
673 Holland, F., Kita, K., Kondo, Y., Li, X., Lou, S. R., Shao, M., Zeng, L. M., Wahner, A., and
674 Zhang, Y. H.: Amplified Trace Gas Removal in the Troposphere, Science, 324, 1702-
675 1704, 10.1126/science.1164566, 2009.
676 Horstjann, M., Andres Hernandez, M. D., Nenakhov, V., Chrobry, A., and Burrows, J.
677 P.: Peroxy radical detection for airborne atmospheric measurements using cavity
678 ehnaced absorption spectroscopy of NO2, Atmospheric Measurement Techniques
679 Discussion, 6, 9655-9688, 2013.
680 Huang, M., Bowman, K. W., Carmichael, G. R., Pierce, R. B., Worden, H. M., Luo, M.,
681 Cooper, O. R., Pollack, I. B., Ryerson, T. B., and Brown, S. S.: Impact of Southern
682 California anthropogenic emissions on ozone pollution in the mountain states:
683 Model analysis and observational evidence from space, J Geophys Res-Atmos, 118,
684 12784-12803, Doi 10.1002/2013jd020205, 2013.
685 Karl, T., Harley, P., Emmons, L., Thornton, B., Guenther, A., Basu, C., Turnipseed, A.,
686 and Jardine, K.: Efficient Atmospheric Cleansing of Oxidized Organic Trace Gases by
687 Vegetation, Science, 330, 816-819, Doi 10.1126/Science.1192534, 2010.

688 Kim, K. H., Ho, D. X., Park, C. G., Ma, C. J., Pandey, S. K., Lee, S. C., Jeong, H. J., and Lee, S.
689 H.: Volatile Organic Compounds in Ambient Air at Four Residential Locations in
690 Seoul, Korea, Environ Eng Sci, 29, 875-889, Doi 10.1089/Ees.2011.0280, 2012.
691 Kim, S., Karl, T., Guenther, A., Tyndall, G., Orlando, J., Harley, P., Rasmussen, R., and
692 Apel, E.: Emissions and ambient distributions of Biogenic Volatile Organic
693 Compounds (BVOC) in a ponderosa pine ecosystem: interpretation of PTR-MS mass
694 spectra, Atmos Chem Phys, 10, 1759-1771, 2010.
695 Kim, S., Guenther, A., Karl, T., and Greenberg, J.: Contributions of primary and
696 secondary biogenic VOC tototal OH reactivity during the CABINEX (Community
697 Atmosphere-Biosphere INteractions Experiments)-09 field campaign, Atmos Chem
698 Phys, 11, 8613-8623, 2011.
699 Kim, S., Guenther, A., and Apel, E.: Quantitative and qualitative sensing techniques
700 for biogenic volatile organic compounds and their oxidation products, Environ Sci-
701 Proc Imp, 15, 1301-1314, Doi 10.1039/C3em00040k, 2013a.
702 Kim, S., Lee, M., Kim, S., Choi, S., Seok, S., and Kim, S.: Photochemical characteristics
703 of high and low ozone episodes observed in the Taehwa Forest observatory (TFO) in
704 June 2011 near Seoul South Korea, Asia-Pacific Journal of Atmospheric Sciences, 49,
705 325-331, Doi 10.1007/S13143-013-0031-0, 2013b.
706 Kim, S., Wolfe, G. M., Mauldin, L., Cantrell, C., Guenther, A., Karl, T., Turnipseed, A.,
707 Greenberg, J., Hall, S. R., Ullmann, K., Apel, E., Hornbrook, R., Kajii, Y., Nakashima, Y.,
708 Keutsch, F. N., DiGangi, J. P., Henry, S. B., Kaser, L., Schnitzhofer, R., Graus, M., Hansel,
709 A., Zheng, W., and Flocke, F. F.: Evaluation of HOx sources and cycling using
710 measurement-constrained model calculations in a 2-methyl-3-butene-2-ol (MBO)
711 and monoterpene (MT) dominated ecosystem, Atmos Chem Phys, 13, 2031-2044,
712 Doi 10.5194/Acp-13-2031-2013, 2013c.
713 Kim, S., VandenBoer, T. C., Young, C. J., Riedel, T. P., Thornton, J. A., Swarthout, B.,
714 Sive, B., Lerner, B., Gilman, J. B., Warneke, C., Roberts, J. M., Guenther, A., Wagner, N.
715 L., Dube, W. P., Williams, E., and Brown, S. S.: The primary and recycling sources of
716 OH during the NACHTT-2011 campaign: HONO as an important OH primary source
717 in the wintertime, J Geophys Res-Atmos, 119, 6886-6896, Doi
718 10.1002/2013jd019784, 2014.
719 Kim, S. Y., Jiang, X. Y., Lee, M., Turnipseed, A., Guenther, A., Kim, J. C., Lee, S. J., and
720 Kim, S.: Impact of biogenic volatile organic compounds on ozone production at the
721 Taehwa Research Forest near Seoul, South Korea, Atmos Environ, 70, 447-453, Doi
722 10.1016/J.Atmosenv.2012.11.005, 2013d.
723 Lelieveld, J., Butler, T. M., Crowley, J. N., Dillon, T. J., Fischer, H., Ganzeveld, L., Harder,
724 H., Lawrence, M. G., Martinez, M., Taraborrelli, D., and Williams, J.: Atmospheric
725 oxidation capacity sustained by a tropical forest, Nature, 452, 737-740, 2008.
726 Levy, H.: Normal Atmosphere - Large Radical and Formaldehyde Concentrations
727 Predicted, Science, 173, 141-143, 1971.
728 Li, X., Brauers, T., Haseler, R., Bohn, B., Fuchs, H., Hofzumahaus, A., Holland, F., Lou,
729 S., Lu, K. D., Rohrer, F., Hu, M., Zeng, L. M., Zhang, Y. H., Garland, R. M., Su, H., Nowak,
730 A., Wiedensohler, A., Takegawa, N., Shao, M., and Wahner, A.: Exploring the
731 atmospheric chemistry of nitrous acid (HONO) at a rural site in Southern China,
732 Atmos Chem Phys, 12, 1497-1513, Doi 10.5194/Acp-12-1497-2012, 2012.

733 Li, Y., Lau, A. K. H., Fung, J. C. H., Zheng, J. Y., and Liu, S. C.: Importance of NOx control
734 for peak ozone reduction in the Pearl River Delta region, J Geophys Res-Atmos, 118,
735 9428-9443, Doi 10.1002/Jgrd.50659, 2013.
736 Lim, Y. J., Armendariz, A., Son, Y. S., and Kim, J. C.: Seasonal variations of isoprene
737 emissions from five oak tree species in East Asia, Atmos Environ, 45, 2202-2210, Doi
738 10.1016/J.Atmosenv.2011.01.066, 2011.
739 Liu, Y. J., Herdlinger-Blatt, I., McKinney, K. A., and Martin, S. T.: Production of methyl
740 vinyl ketone and methacrolein via the hydroperoxyl pathway of isoprene oxidation,
741 Atmos Chem Phys, 13, 5715-5730, Doi 10.5194/Acp-13-5715-2013, 2013.
742 Lou, S., Holland, F., Rohrer, F., Lu, K., Bohn, B., Brauers, T., Chang, C. C., Fuchs, H.,
743 Haseler, R., Kita, K., Kondo, Y., Li, X., Shao, M., Zeng, L., Wahner, A., Zhang, Y., Wang,
744 W., and Hofzumahaus, A.: Atmospheric OH reactivities in the Pearl River Delta -
745 China in summer 2006: measurement and model results, Atmos Chem Phys, 10,
746 11243-11260, 2010.
747 Lu, K. D., Rohrer, F., Holland, F., Fuchs, H., Bohn, B., Brauers, T., Chang, C. C., Haseler,
748 R., Hu, M., Kita, K., Kondo, Y., Li, X., Lou, S. R., Nehr, S., Shao, M., Zeng, L. M., Wahner,
749 A., Zhang, Y. H., and Hofzumahaus, A.: Observation and modelling of OH and HO2
750 concentrations in the Pearl River Delta 2006: a missing OH source in a VOC rich
751 atmosphere, Atmos Chem Phys, 12, 1541-1569, Doi 10.5194/Acp-12-1541-2012,
752 2012.
753 Ma, J. Z., Wang, W., Chen, Y., Liu, H. J., Yan, P., Ding, G. A., Wang, M. L., Sun, J., and
754 Lelieveld, J.: The IPAC-NC field campaign: a pollution and oxidization pool in the
755 lower atmosphere over Huabei, China, Atmos Chem Phys, 12, 3883-3908, Doi
756 10.5194/Acp-12-3883-2012, 2012.
757 Mao, J., Ren, X., Zhang, L., Van Duin, D. M., Cohen, R. C., Park, J. H., Goldstein, A. H.,
758 Paulot, F., Beaver, M. R., Crounse, J. D., Wennberg, P. O., DiGangi, J. P., Henry, S. B.,
759 Keutsch, F. N., Park, C., Schade, G. W., Wolfe, G. M., Thornton, J. A., and Brune, W. H.:
760 Insights into hydroxyl measurements and atmospheric oxidation in a California
761 forest, Atmos Chem Phys, 12, 8009-8020, Doi 10.5194/Acp-12-8009-2012, 2012.
762 Mao, J. Q., Ren, X. R., Chen, S. A., Brune, W. H., Chen, Z., Martinez, M., Harder, H., Lefer,
763 B., Rappengluck, B., Flynn, J., and Leuchner, M.: Atmospheric oxidation capacity in
764 the summer of Houston 2006: Comparison with summer measurements in other
765 metropolitan studies, Atmos Environ, 44, 4107-4115, Doi
766 10.1016/J.Atmosenv.2009.01.013, 2010.
767 Na, K., and Kim, Y. P.: Seasonal characteristics of ambient volatile organic
768 compounds in Seoul, Korea, Atmos Environ, 35, 2603-2614, Doi 10.1016/S1352-
769 2310(00)00464-7, 2001.
770 Nakashima, Y., Kato, S., Greenberg, J., Harley, P., Karl, T., Turnipseed, A., Apel, E.,
771 Guenther, A., Smith, J., and Kajii, Y.: Total OH reactivity measurements in ambient air
772 in a southern Rocky mountain ponderosa pine forest during BEACHON-SRM08
773 summer campaign, Atmos Environ, 85, 1-8, Doi 10.1016/J.Atmosenv.2013.11.042,
774 2014.
775 NIER: Annual Report for Atmospheric Environment, National Insititute of
776 Environmetal Rsearch, 2010.
777 Nolscher, A. C., Williams, J., Sinha, V., Custer, T., Song, W., Johnson, A. M., Axinte, R.,
778 Bozem, H., Fischer, H., Pouvesle, N., Phillips, G., Crowley, J. N., Rantala, P., Rinne, J.,

779 Kulmala, M., Gonzales, D., Valverde-Canossa, J., Vogel, A., Hoffmann, T., Ouwersloot,
780 H. G., de Arellano, J. V. G., and Lelieveld, J.: Summertime total OH reactivity
781 measurements from boreal forest during HUMPPA-COPEC 2010, Atmos Chem Phys,
782 12, 8257-8270, Doi 10.5194/Acp-12-8257-2012, 2012.
783 Oswald, R., Behrendt, T., Ermel, M., Wu, D., Su, H., Cheng, Y., Breuninger, C., Moravek,
784 A., Mougin, E., Delon, C., Loubet, B., Pommerening-Roser, A., Sorgel, M., Poschl, U.,
785 Hoffmann, T., Andreae, M. O., Meixner, F. X., and Trebs, I.: HONO Emissions from Soil
786 Bacteria as a Major Source of Atmospheric Reactive Nitrogen, Science, 341, 1233-
787 1235, Doi 10.1126/Science.1242266, 2013.
788 Paulot, F., Crounse, J. D., Kjaergaard, H. G., Kroll, J. H., Seinfeld, J. H., and Wennberg, P.
789 O.: Isoprene photooxidation: new insights into the production of acids and organic
790 nitrates, Atmos Chem Phys, 9, 1479-1501, 2009.
791 Paulson, S. E., and Seinfeld, J. H.: Development and evaluation of a photooxidation
792 mechanism for isoprene, Journal of Geophysical Research, 97, 20703-20715, 1992.
793 Peeters, J., and Muller, J. F.: HOx radical regeneration in isoprene oxidation via
794 peroxy radical isomerisations. II: experimental evidence and global impact, Phys
795 Chem Chem Phys, 12, 14227-14235, Doi 10.1039/C0cp00811g, 2010.
796 Pollack, I. B., Ryerson, T. B., Trainer, M., Neuman, J. A., Roberts, J. M., and Parrish, D.
797 D.: Trends in ozone, its precursors, and related secondary oxidation products in Los
798 Angeles, California: A synthesis of measurements from 1960 to 2010, J Geophys Res-
799 Atmos, 118, 5893-5911, Doi 10.1002/Jgrd.50472, 2013.
800 Ran, L., Zhao, C. S., Xu, W. Y., Lu, X. Q., Han, M., Lin, W. L., Yan, P., Xu, X. B., Deng, Z. Z.,
801 Ma, N., Liu, P. F., Yu, J., Liang, W. D., and Chen, L. L.: VOC reactivity and its effect on
802 ozone production during the HaChi summer campaign, Atmos Chem Phys, 11, 4657-
803 4667, Doi 10.5194/Acp-11-4657-2011, 2011.
804 Ren, X., Sanders, J. E., Rajendran, A., Weber, R. J., Goldstein, A. H., Pusede, S. E.,
805 Browne, E. C., Min, K. E., and Cohen, R. C.: A relaxed eddy accumulation system for
806 measuring vertical fluxes of nitrous acid, Atmos Meas Tech, 4, 2093-2103, Doi
807 10.5194/Amt-4-2093-2011, 2011.
808 Ryerson, T. B., Andrews, A. E., Angevine, W. M., Bates, T. S., Brock, C. A., Cairns, B.,
809 Cohen, R. C., Cooper, O. R., de Gouw, J. A., Fehsenfeld, F. C., Ferrare, R. A., Fischer, M.
810 L., Flagan, R. C., Goldstein, A. H., Hair, J. W., Hardesty, R. M., Hostetler, C. A., Jimenez, J.
811 L., Langford, A. O., McCauley, E., McKeen, S. A., Molina, L. T., Nenes, A., Oltmans, S. J.,
812 Parrish, D. D., Pederson, J. R., Pierce, R. B., Prather, K., Quinn, P. K., Seinfeld, J. H.,
813 Senff, C. J., Sorooshian, A., Stutz, J., Surratt, J. D., Trainer, M., Volkamer, R., Williams, E.
814 J., and Wofsy, S. C.: The 2010 California Research at the Nexus of Air Quality and
815 Climate Change (CalNex) field study, J Geophys Res-Atmos, 118, 5830-5866, Doi
816 10.1002/Jgrd.50331, 2013.
817 Ryu, Y. H., Baik, J. J., Kwak, K. H., Kim, S., and Moon, N.: Impacts of urban land-surface
818 forcing on ozone air quality in the Seoul metropolitan area, Atmos Chem Phys, 13,
819 2177-2194, Doi 10.5194/Acp-13-2177-2013, 2013.
820 Sartelet, K. N., Couvidat, F., Seigneur, C., and Roustan, Y.: Impact of biogenic
821 emissions on air quality over Europe and North America, Atmos Environ, 53, 131-
822 141, Doi 10.1016/J.Atmosenv.2011.10.046, 2012.
823 Seinfeld, J. H.: Urban Air-Pollution - State of the Science, Science, 243, 745-752, Doi
824 10.1126/Science.243.4892.745, 1989.

825 Shao, M., Lu, S. H., Liu, Y., Xie, X., Chang, C. C., Huang, S., and Chen, Z. M.: Volatile
826 organic compounds measured in summer in Beijing and their role in ground-level
827 ozone formation, J Geophys Res-Atmos, 114, Artn D00g06
828 Doi 10.1029/2008jd010863, 2009a.
829 Shao, M., Zhang, Y. H., Zeng, L. M., Tang, X. Y., Zhang, J., Zhong, L. J., and Wang, B. G.:
830 Ground-level ozone in the Pearl River Delta and the roles of VOC and NO(x) in its
831 production, J Environ Manage, 90, 512-518, Doi 10.1016/J.Jenvman.2007.12.008,
832 2009b.
833 Sillman, S., and He, D.: Some theoretical results concerning O3-NOx-VOC chemistry
834 and NOx-VOC indicators, Journal of Geophysical Research, 107,
835 4659,doi:4610.1029:2001JD001123, 2002.
836 Sinha, V., Williams, J., Lelieveld, J., Ruuskanen, T. M., Kajos, M. K., Patokoski, J., Hellen,
837 H., Hakola, H., Mogensen, D., Boy, M., Rinne, J., and Kulmala, M.: OH Reactivity
838 Measurements within a Boreal Forest: Evidence for Unknown Reactive Emissions,
839 Environ Sci Technol, 44, 6614-6620, Doi 10.1021/Es101780b, 2010.
840 Song, C. H., Park, M. E., Lee, E. J., Lee, J. H., Lee, B. K., Lee, D. S., Kim, J., Han, J. S., Moon,
841 K. J., and Kondo, Y.: Possible particulate nitrite formation and its atmospheric
842 implications inferred from the observations in Seoul, Korea, Atmos Environ, 43,
843 2168-2173, Doi 10.1016/J.Atmosenv.2009.01.018, 2009.
844 Spaulding, R. S., Schade, G. W., Goldstein, A. H., and Charles, M. J.: Characterization of
845 secondary atmospheric photooxidation products: Evidence for biogenic and
846 anthropogenic sources, J Geophys Res-Atmos, 108, Artn 4247
847 Doi 10.1029/2002jd002478, 2003.
848 Tie, X., Geng, F., Guenther, A., Cao, J., Greenberg, J., Zhang, R., Apel, E., Li, G.,
849 Weinheimer, A., Chen, J., and Cai, C.: Megacity impacts on regional ozone formation:
850 observations and WRF-Chem modeling for the MIRAGE-Shanghai field campaign,
851 Atmos Chem Phys, 13, 5655-5669, Doi 10.5194/Acp-13-5655-2013, 2013.
852 Tonnesen, G. S., and Dennis, R. L.: Analysis of radical propagation efficiency to assess
853 ozone sensitivity to hydrocarbons and NOx 1. Local indicators of instantaneous odd
854 oxygen production sensitivity, J Geophys Res-Atmos, 105, 9213-9225, Doi
855 10.1029/1999jd900371, 2000a.
856 Tonnesen, G. S., and Dennis, R. L.: Analysis of radical propagation efficiency to assess
857 ozone sensitivity to hydrocarbons and NOx 2. Long-lived species as indicators of
858 ozone concentration sensitivity, J Geophys Res-Atmos, 105, 9227-9241, Doi
859 10.1029/1999jd900372, 2000b.
860 Trainer, M., Williams, E., Parrish, D. D., Buhr, M. P., Allwine, E. J., Westberg, H.,
861 Fehsenfeld, F. C., and Liu, S. C.: Models and observations of the impact of natural
862 hydrocarbons on rural ozone, Nature, 329, 705 - 707, 1987.
863 Tseng, K. H., Wang, J. L., Cheng, M. T., and Tsuang, B. J.: Assessing the Relationship
864 between Air Mass Age and Summer Ozone Episodes Based on Photochemical
865 Indices, Aerosol Air Qual Res, 9, 149-171, 2009.
866 VandenBoer, T., Murphy, J. G., Roberts, J. M., Middlebrook, A. M., Brock, C., Lerner, B.
867 M., Wolfe, D. E., Williams, E., Brown, S. S., Warneke, C., De Gouw, J., Wagner, N. L.,
868 Young, C. C., Dube, W. P., Bahreini, R., Riedel, T., Thornton, J. A., Ozturk, F., Keene, W.,
869 Maben, J. R., Pszenny, A., Kim, S., Grossberg, N., and Lefer, B.: Understanding the role

of the ground surface in HONO vertical structure: High resolution vertical profiles during NACHTT-11, submitted, 2013.
Wolfe, G. M., and Thornton, J. A.: The chemistry of atmosphere-forest exchange (CAFE) model - PART1: Model description and characterization, Atmos Chem Phys, 11, 77-101, 2011.
Wolfe, G. M., Thornton, J. A., Bouvier-Brown, N. C., Goldstein, A. H., Park, J. H., Mckay, M., Matross, D. M., Mao, J., Brune, W. H., LaFranchi, B. W., Browne, E. C., Min, K. E., Wooldridge, P. J., Cohen, R. C., Crounse, J. D., Faloona, I. C., Gilman, J. B., Kuster, W. C., de Gouw, J. A., Huisman, A., and Keutsch, F. N.: The Chemistry of Atmosphere-Forest Exchange (CAFE) Model - Part 2: Application to BEARPEX-2007 observations, Atmos Chem Phys, 11, 1269-1294, Doi 10.5194/Acp-11-1269-2011, 2011.
Wolfe, G. M., Crounse, J. D., Parrish, J. D., St Clair, J. M., Beaver, M. R., Paulot, F., Yoon, T. P., Wennberg, P. O., and Keutsch, F. N.: Photolysis, OH reactivity and ozone reactivity of a proxy for isoprene-derived hydroperoxyenals (HPALDs), Phys Chem Chem Phys, 14, 7276-7286, 2012.
Wolfe, G. M., Cantrell, C., Kim, S., Mauldin, R., Karl, T., Harley, P., Turnipseed, A., Zheng, W., Flocke, F., Apel, E., Hornbrook, R. S., Hall, S., Ullmann, K., Henry, S. B., Digangi, J., Boyle, E. S., Kaser, L., Schnitzhofer, R., Hansel, A., Graus, M., Nakashima, Y., Kajii, Y., Guenther, A., and Keutsch, F.: Missing peroxy radical sources within a rural forest canopy, Atmospheric Chemistry and Physics Discussion, 13, 31713-31759, 2013.
Wong, K. W., Tsai, C., Lefer, B., Haman, C., Grossberg, N., Brune, W. H., Ren, X., Luke, W., and Stutz, J.: Daytime HONO vertical gradients during SHARP 2009 in Houston, TX, Atmos Chem Phys, 12, 635-652, Doi 10.5194/Acp-12-635-2012, 2012.
Xing, J., Wang, S. X., Jang, C., Zhu, Y., and Hao, J. M.: Nonlinear response of ozone to precursor emission changes in China: a modeling study using response surface methodology, Atmos Chem Phys, 11, 5027-5044, Doi 10.5194/Acp-11-5027-2011, 2011.
Yoshino, A., Nakashima, Y., Miyazaki, K., Kato, S., Suthawaree, J., Shimo, N., Matsunaga, S., Chatani, S., Apel, E., Greenberg, J., Guenther, A., Ueno, H., Sasaki, H., Hoshi, J., Yokota, H., Ishii, K., and Kajii, Y.: Air quality diagnosis from comprehensive observations of total OH reactivity and reactive trace species in urban central Tokyo, Atmos Environ, 49, 51-59, Doi 10.1016/J.Atmosenv.2011.12.029, 2012.
Zhang, Y., Hu, X. M., Leung, L. R., and Gustafson, W. I.: Impacts of regional climate change on biogenic emissions and air quality, J Geophys Res-Atmos, 113, Artn D18310
Doi 10.1029/2008jd009965, 2008a.
Zhang, Y. H., Su, H., Zhong, L. J., Cheng, Y. F., Zeng, L. M., Wang, X. S., Xiang, Y. R., Wang, J. L., Gao, D. F., Shao, M., Fan, S. J., and Liu, S. C.: Regional ozone pollution and observation-based approach for analyzing ozone-precursor relationship during the PRIDE-PRD2004 campaign, Atmos Environ, 42, 6203-6218, Doi 10.1016/J.Atmosenv.2008.05.002, 2008b.
Zhao, J., and Zhang, R. Y.: Proton transfer reaction rate constants between hydronium ion (H3O(+)) and volatile organic compounds, Atmos Environ, 38, 2177-2185, 2004.

915 Zhou, X. L., Zhang, N., TerAvest, M., Tang, D., Hou, J., Bertman, S., Alaghmand, M.,
916 Shepson, P. B., Carroll, M. A., Griffith, S., Dusanter, S., and Stevens, P. S.: Nitric acid
917 photolysis on forest canopy surface as a source for tropospheric nitrous acid, Nat
918 Geosci, 4, 440-443, Doi 10.1038/Ngeo1164, 2011.

919
920

921 Table 1. Analytical characteristics of trace gas analyzers at TRF

922

Chemical Species	Manufacturer and Model Number	Uncertainty	Lower Limit of Detection
CO	Thermo Scientific 48i TLE	10%	40 ppb
NO_X	Thermo Scientific 42i-TL	15%	50 ppt
SO_2	Thermo Scientific 43i-TLE	10%	50 ppt
ozone	Thermo Scientific 49i	5%	< 1 ppb

923
924

925

926 Table 2. Terpenoid speciation analysis results from GC-MS a) branch enclosure and b)
927 ambient air samples.

928

929 a)

Terpenoids	*Composition(%)	Speciation	*Composition(%)
Isoprene	0.5		
Monoterpenes	92.9	α-pinene	36.7
		camphene	13.1
		β-pinene	12.0
		β-myrcene	27.7
		α-terpinolene	1.9
		d-limonene	8.6
Sesquiterpenes	6.6	β-caryophyllene	53.2
		α-caryophyllene	46.8

930

931 b)

Terpeniods	*Composition(%)	Speciation	*Composition(%)
Monoterpenes	98.6	α-pinene	38.8
		β-piene	36.5
		camphene	13.5
		d-limonene	11
Sesquiterpenes	1.4	longifolene	100

932 *Composition is calculated based on the mixing ratio scale

933
934

Table 3. A summary of critical differences in input parameters for four different model simulation scenarios presented in this study

	HPALD chemistry	*α	Observational Constraints
Scenario I	No	0	-All
Scenario II	#Peeters and Muller (2010)	0	-All
Scenario III	+Crounse et al. (2011)	0	-All
Scenario IV	#Peeters and Muller (2010)	2.6	-All
Scenario V	+Crounse et al. (2011)	2.6	-All
Scenario VI	#Peeters and Muller (2010)	2.6	-All but HONO

*α is an OH yield from reactions between an isoprene peroxy radical and HO_2, #k298 = ~ 0.08 for isoprene peroxy radical isomerization rate leading to produce HPALD, +k298 = 0.002 for isoprene peroxy radical isomerization rate, - All the observed diurnal variations, appeared in Figure 1 are constrained in the model along with ambient pressure and humidity.

963 Table 4 A summary for radical distributions from the observationally constrained box-
964 model simulation results
965

	OH		HO_2		RO_2		Constraints
Local Time	8:00-12:00	13:00-16:00	8:00-12:00	13:00-16:00	8:00-12:00	13:00-16:00	
Scenario I	3.85×10^6	3.08×10^6	4.10×10^8	7.02×10^8	3.65×10^8	1.14×10^9	All
Scenario II	3.99×10^6	3.69×10^6	3.99×10^8	7.86×10^8	3.51×10^8	9.62×10^8	All
Scenario III	3.86×10^6	3.13×10^6	4.09×10^8	7.09×10^8	3.64×10^8	1.12×10^9	All
Scenario IV	4.27×10^6	4.49×10^6	4.29×10^8	8.70×10^8	3.66×10^8	1.06×10^9	All
Scenario V	4.21×10^6	4.52×10^6	4.55×10^8	8.55×10^8	3.86×10^8	1.28×10^9	All
Scenario VI	1.61×10^6	1.61×10^6	1.95×10^8	4.82×10^8	1.75×10^8	7.25×10^8	All but HONO
Scenario VII	1.82×10^6	2.55×10^6	2.09×10^8	6.07×10^8	1.80×10^8	7.00×10^8	All but HONO

966 unit: molecules cm^{-3}
967
968

Figure 1. Averaged temporal variations observed trace gases and ambient temperature at TRF (June 1st to June 6th, 2012, KST stands for Korean Standard Time GMT+9). The uncertainty for each observable is listed in the main text.

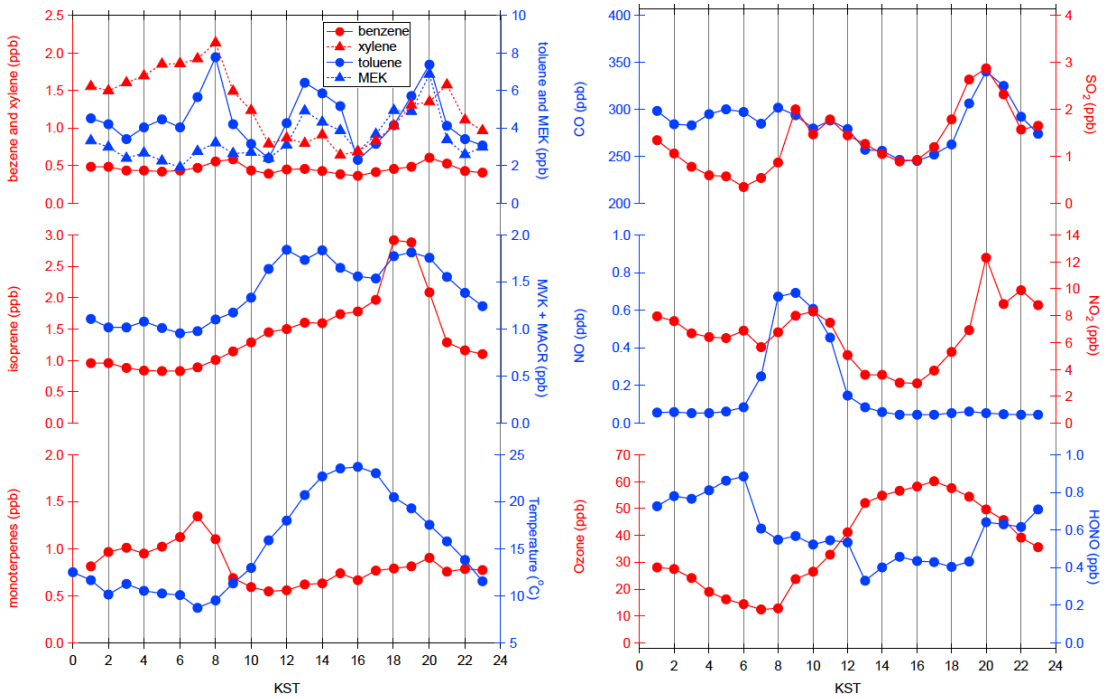

977 Figure 2. The temporal variations of OH reactivity calculated from the observed dataset
978 at TRF (Figure 1).
979
980

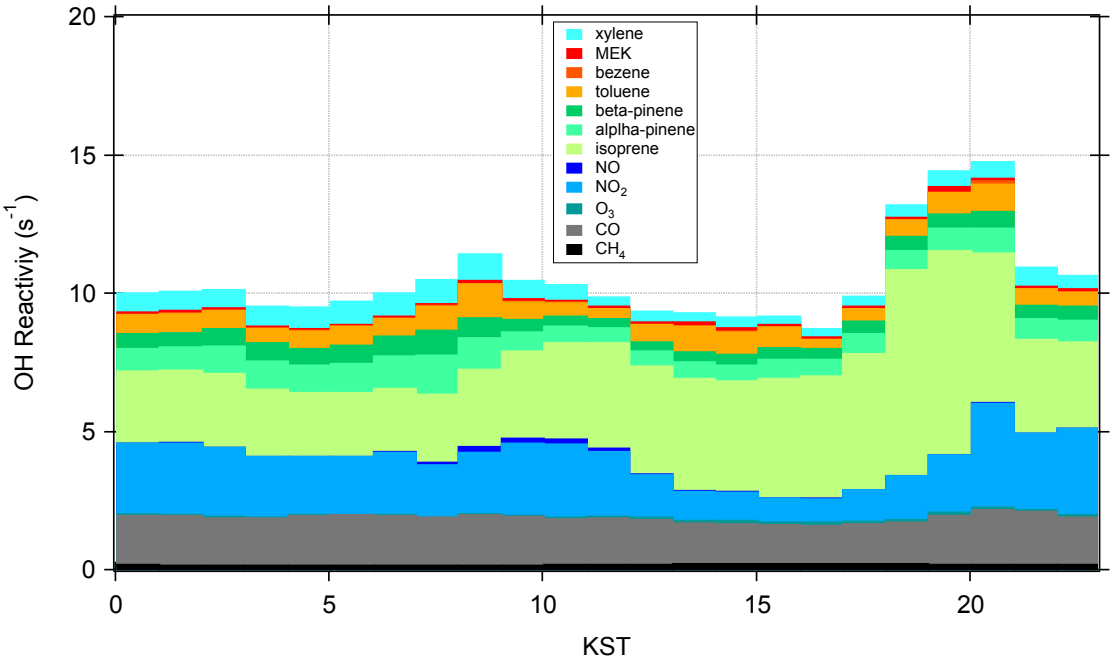

981
982
983
984

Figure 3. The temporal variations of OH (a) and d)), HO_2 (b) and e), and RO_2 (c) and f)) calculated by six different observationally constrained UWCM box model scenarios.

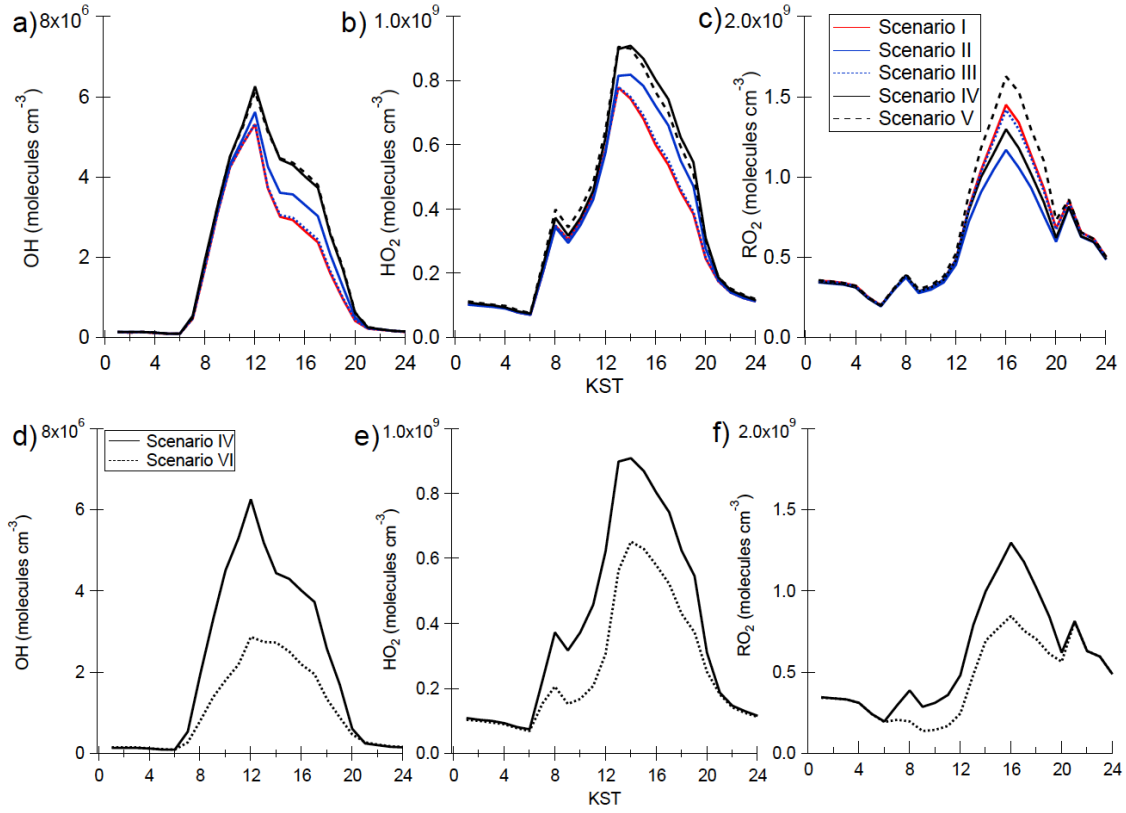

Figure 4 The temporal variations of radical recycling (red) and destruction (blue, black and green) rates calculated using the UWCM box model for different model scenarios

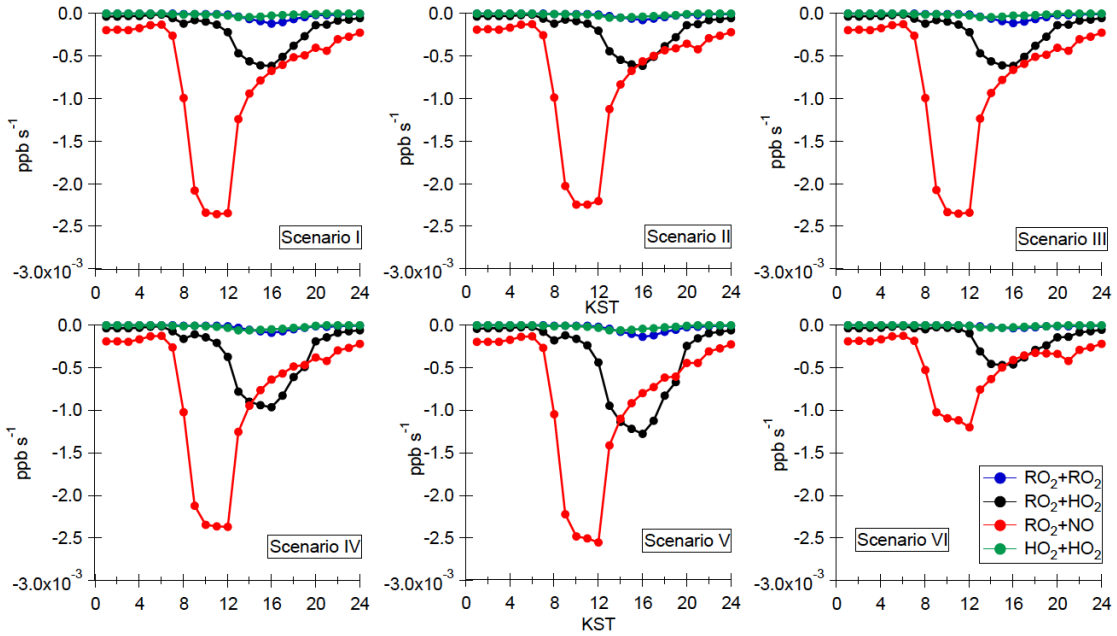

Figure 5. The temporal variations of P_{H2O2}/P_{HNO3} calculated from the UWCM box model from six different model scenarios

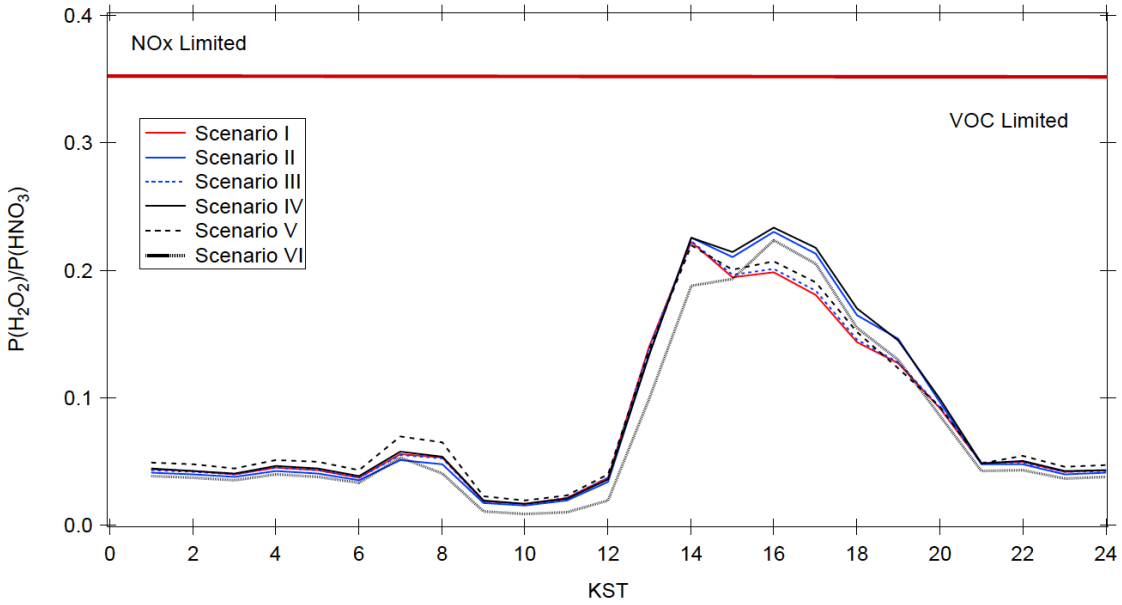

Figure 6. The temporal distributions of UWCM calculated OH reactivity (a) and formaldehyde (b)